# Improved magnetization and reduced leakage current in Sm and Sc co-substituted $BiFeO_3$

T. Durga Rao, Kumara Raja Kandula, Abhinav Kumar, and Saket Asthana

Citation: Journal of Applied Physics **123**, 244104 (2018); doi: 10.1063/1.5023720

View online: https://doi.org/10.1063/1.5023720

View Table of Contents: http://aip.scitation.org/toc/jap/123/24

Published by the American Institute of Physics



# Improved magnetization and reduced leakage current in Sm and Sc co-substituted $BiFeO_3$

T. Durga Rao,[1,2,a)] Kumara Raja Kandula,[1] Abhinav Kumar,[1] and Saket Asthana[1,a)]
[1]*Advanced Functional Materials Laboratory, Department of Physics, Indian Institute of Technology Hyderabad, Telangana, India*
[2]*Department of Physics, Institute of Science, GITAM University, Visakhapatnam, Andhra Pradesh-530045, India*

(Received 27 January 2018; accepted 5 June 2018; published online 28 June 2018)

$BiFeO_3$ (BFO) and $Bi_{0.85}Sm_{0.15}Fe_{0.90}Sc_{0.10}O_3$ (BSFSO) ceramics were synthesized by conventional solid state route. X-ray diffraction measurements revealed that an orthorhombic *Pnma* structure evolved with a phase fraction of 84% in the rhombohedral *R3c* structure of BFO upon the substitution of Sm and Sc. The changes in the intensity and the frequency of Raman modes also corroborated the structural transformation in the BSFSO compound. A decrease in grain size, reduction in porosity, and improved density were observed in the BSFSO compound. An enhanced remanent magnetization of 0.2 emu/g and coercive field of 6.2 kOe were observed, which were attributed to the structural change as well as the destruction of the spin structure with the substitution. Impedance and leakage current measurements revealed that the insulating character of BFO was improved with the substitution of Sm and Sc in BFO and was explained based on the bond enthalpy concept. The enhanced magnetic properties along with the improved insulating character of BSFSO compound will be suitable for device applications. *Published by AIP Publishing.*
https://doi.org/10.1063/1.5023720

## INTRODUCTION

Multiferroics refer to a class of materials which exhibit more than one ferroic order in the same phase.[1] They have attracted great attention owing to their potential for application in next generation memory devices, spintronics, magnetic sensors, etc.[2] However, the potential of these materials for room temperature device applications is limited as most of the known single phase multiferroics show their magnetic transition temperatures below room temperature.[3,4] $BiFeO_3$ (BFO) has become one of the most widely studied multiferroic so far because of its high ferroelectric Curie temperature ($T_C = 830\,^{\circ}C$) and Neel temperature ($T_N = 370\,^{\circ}C$).[5] BFO, in its bulk form, exhibits a rhombohedral structure with *R3c* space group. The coupling between spin and charge in it would have an additional degree of freedom of changing magnetization by the electric field and vice versa.[6] The ferroelectricity originates due to the hybridization of $6s^2$ lone pair electrons of $Bi^{3+}$ ions with the $2p^6$ electrons of $O^{2-}$ ions. The magnetic behavior of BFO is due to the partially filled *3d* orbital electrons of $Fe^{3+}$ ions which align in the *G*-type antiferromagnetic structure.[7] However, the potential of BFO for practical application is hindered because of the major issues including the formation of impurity phases, appearance of weak ferromagnetism, and the presence of high leakage currents which limit the BFO for its practical application.[5,8] The high leakage currents are attributed to the mixed valence states of Fe (i.e., $Fe^{2+}/Fe^{3+}$) which in turn promote the formation of oxygen vacancies[9] as explained by using the following equation:

$$2Fe^{3+} + O^{2-} \Rightarrow 2Fe^{2+} + V_O^{\bullet\bullet} + \frac{1}{2}O_2, \tag{1}$$

where $V_o^{\bullet\bullet}$ is the oxygen vacancy.

The leakage current may be reduced by substituting a suitable element (say *R*) at *A*/*B*-sites. It is reported that the stronger bond enthalpy of the R-O bond than those of Bi/Fe-O bonds will facilitate to recover the oxygen vacancies and consequently reduces the leakage current. It has been observed that the substitution of Sc at the Fe-site of BFO enhances the insulating character by reducing the leakage current.[10,11] Also, it is reported that rare earth substitution at Bi-site enhances the multiferroic properties and reduces the leakage currents.[11,12] In addition to the improved properties, the substitution distorts the crystal structure and transforms to another structure. A structural transition from rhombohedral to an orthorhombic structure is observed for $0.10 < x < 0.15$ in the $Bi_{1-x}Eu_xFeO_3$ compound.[13] The substitution of $Bi^{3+}$ by $Gd^{3+}$ in $Bi_{1-x}Gd_xFeO_3$ compounds transforms the crystal structure from rhombohedral *R3c* to an orthorhombic $Pn2_1a$ structure up to $x = 0.10$ and then to an orthorhombic *Pnma* structure for $0.20 < x < 0.30$.[14] The rhombohedral structure of BFO persists up to $x = 0.10$ and evolution of orthorhombic phase was observed for $x > 0.15$ in $Bi_{1-x}Ho_xFeO_3$ compounds.[15] It is observed that the substitution of $Sm^{3+}$ at Bi-site has drawn considerable attention due to its ability to enhance the multiferroic properties.[16] It was predicted using first principles calculations that a morphotropic phase boundary of rhombohedral (*R3c*) and

a)Authors to whom correspondence should be addressed: durgarao.tadisetti@gitam.edu and asthanas@iith.ac.in

orthorhombic (*Pnma*) phases exists for $x = 0.14$ in $Bi_{1-x}Sm_xFeO_3$ compounds.[17] The substitution of $Bi^{3+}$ by $Sm^{3+}$ in BFO above 14 mol. % may change the structure to orthorhombic with *Pnma* phase. The structural distortions change the Fe-O-Fe bond angles and Fe-O bond distances which in turn modify the magnetic interactions. Based on the above discussion, it can be anticipated that the co-substitution of Sm at the Bi-site and Sc at the Fe-site would improve the magnetic properties along with reduced leakage currents. In the present work, polycrystalline $BiFeO_3$ and $Bi_{0.85}Sm_{0.15}$ $Fe_{0.90}Sc_{0.10}O_3$ compounds were synthesized and their structural, magnetic, impedance, and electrical properties were analyzed and compared with BFO.

## EXPERIMENTAL DETAILS

Polycrystalline BFO and BSFSO compounds were synthesized by conventional solid-state reaction technique. The detailed experimental analysis can be found elsewhere.[10] The structural analysis was carried out by an X-ray diffractometer (Panalytical X'pert Pro) with $CuK_\alpha$ radiation ($\lambda = 1.5406$ Å) in the range $20° \leq 2\theta \leq 90°$. The microstructural analysis was performed using field emission scanning electron microscopy (FE-SEM, Carl Zeiss, Supra 40). Raman scattering spectra were measured using a laser micro-Raman spectrometer (Bruker, Senterra) with an excitation source of 785 nm. The room temperature magnetic properties were measured up to a field of 50 kOe using physical property measurement system (PPMS) with VSM assembly (Quantum Design, USA). Differential scanning calorimetry (DSC) measurement was performed on a TA-Q200 calorimeter at a heating rate of 10 °C/min under $N_2$ atmosphere. The impedance measurements were performed using a Wayne Kerr 6500B impedance analyser in the temperature range from 30 °C to 400 °C. The leakage current density measurement was carried out using an aixACCT TF 2000 analyzer.

## RESULTS AND DISCUSSIONS

### Structural studies

X-ray diffraction (XRD) patterns of BFO and BSFSO compounds are shown in Fig. 1. A trace amount of impurity phases, such as $Bi_{25}FeO_{40}$ and $Bi_2Fe_4O_9$, are observed. However, the formation of these phases is unavoidable during synthesis of BFO.[18,19] The presence of these impurity phases could not alter the multiferroic properties of BFO as they neither show ferromagnetic nor ferroelectric properties at room temperature.[20] It is evidenced from the XRD pattern that BFO is crystallized in the rhombohedral *R3c* structure whereas prominent structural changes could be observed in the BSFSO compound, which are discussed below.

The two Bragg's reflections (104) and (110) at around $2\theta = 32°$ show variations in their intensities and form as a single broad peak. An evolution of new peak at $2\theta = 22.7°$ and the decrease in the intensity of peak (006) at $2\theta = 39°$ are observed as shown in Fig. 2. All these changes demonstrate that the crystal structure of BFO transforms from a rhombohedral structure to another structure with the co-substitution of Sm and Sc at their respective sites. The Rietveld refinement is

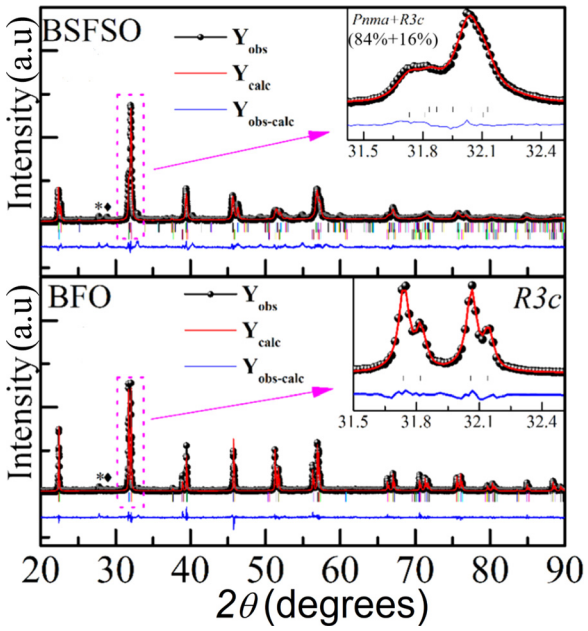


FIG. 1. Room temperature XRD patterns of BFO and BSFSO compounds in the range $20° \leq 2\theta \leq 90°$. The observed data, fitted data, and difference between observed and fitted data are represented by solid black circles, red lines, and blue lines, respectively. * and ◆ represent impurity phases $Bi_{25}FeO_{40}$ and $Bi_2Fe_4O_9$, respectively.

carried out to analyze the crystal structure of the BSFSO compound. The refinement indicates that a mixture of orthorhombic structure with *Pnma* phase and rhombohedral structure with *R3c* phase exists with phase fractions 84% and 16%, respectively, in the compound. The presence of orthorhombic structure with *Pnma* phase is also consistent with the literature.[21,22]

The mixed structures have been reported in various substituted/co-substituted BFO systems.[12,23–25] The evolution of orthorhombic phase can be interpreted using Goldschmidt tolerance factor *t*, which is defined as

$$t = \frac{(\langle r_A \rangle + r_O)}{\sqrt{2}(\langle r_B \rangle + r_O)}, \tag{2}$$

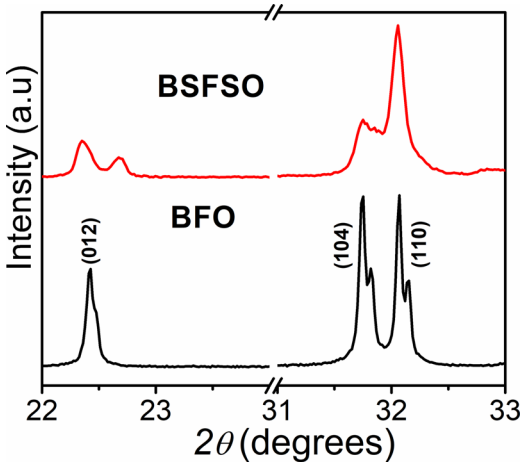


FIG. 2. XRD patterns of BFO and BSFSO compounds in the range $22° \leq 2\theta \leq 32.7°$.

TABLE I. Lattice parameters and position coordinates obtained from Rietveld refinement for BFO and BSFSO compounds.

| BFO (*R3c*) | | | |
|---|---|---|---|
| | *x* | *y* | *z* |
| Bi | 0.0000 | 0.0000 | 0.0000 |
| Fe | 0.0000 | 0.0000 | 0.2207 |
| O | 0.4313 | 0.0017 | 0.9475 |
| Lattice parameters | $a = 5.5790$ Å, $b = 5.5790$ Å, $c = 13.8700$ Å $\alpha = \beta = 90°$, $\gamma = 120°$ | | |
| Fe-O-Fe 153.0(3) | | | |
| $\chi^2 = 2.53$ | | | |

| BSFSO | | | | | | | |
|---|---|---|---|---|---|---|---|
| *Pnma* (84%) | | | | *R3c* (16%) | | | |
| Lattice positions | *x* | *y* | *z* | Lattice positions | *x* | *y* | *z* |
| Bi/Sm | 0.0131 | 0.2500 | 0.9909 | Bi/Sm | 0.0000 | 0.0000 | 0.0000 |
| Fe/Sc | 0.0000 | 0.0000 | 0.5000 | Fe/Sc | 0.0000 | 0.0000 | 0.2229 |
| $O_1$ | 0.4335 | 0.2500 | 0.0873 | O | 0.4431 | 0.0792 | 0.9384 |
| $O_2$ | 0.2370 | 0.5147 | 0.2099 | | | | |
| Lattice parameters | $a = 5.6112$ Å, $b = 7.8369$ Å, $c = 5.6315$ Å $\alpha = \beta = \gamma = 90°$ | | | $a = b = 5.5708$ Å, $c = 13.8841$ Å $\alpha = \beta = 90°$, $\gamma = 120°$ | | | |
| Fe/Sc-O1-Fe/Sc | 145.2(6) | | | 135(5) | | | |
| Fe/Sc-O2-Fe/Sc | 166.1(13) | | | | | | |
| $\chi^2 = 5.28$ | | | | | | | |

where $\langle r_A \rangle$ and $\langle r_B \rangle$ are the average radii at *A*-site and *B*-site, respectively, and $r_o$ is the radius of $O^{2-}$ ions. The co-substitution of the smaller ionic size of $Sm^{3+}$ ions (1.28 Å) at $Bi^{3+}$-site (1.36 Å) and larger ionic size of $Sc^{3+}$ ions (0.745 Å) at $Fe^{3+}$-site (0.645 Å) decreases the tolerance factor *t* according to its definition. The decrease in *t* induces lattice distortion which in turn leads to evolution of lower symmetric phase.[12] The structural distortion modifies Fe(/Sc)-O bond distances and Fe(/Sc)-O-Fe(/Sc) bond angles in the BSFSO compound which leads to changes in physical properties. The presence of major centrosymmetric orthorhombic *Pnma* phase in the BSFSO compound may enhance the magnetic properties by suppressing the spin structure and weaken the ferroelectric/dielectric properties. The lattice parameters, bond distances, bond angles, and position coordinates of BFO and BSFSO compounds are given in Table I.

## Microstructural studies

FE-SEM micrographs of BFO and BSFSO compounds are shown in Fig. 3. The average grain sizes of BFO and BSFSO compounds are 9 and 2 $\mu$m, respectively. The decrease in the grain size of BSFSO compound is consistent with the observation of increase in full width at half maxima (FWHM) of XRD peaks. The reduction in the grain size of BSFSO compound is due to low diffusivity of rare earth elements.[26] Further, the substitution of $Sc^{3+}$ at the Fe-site would reduce the oxygen vacancies due to (i) the stronger bond enthalpy of Sc-O bond (681.6711.3 kJ/mol) than that of Fe-O bond (390.4717.2 kJ/mol)[27] and (ii) stabilization of the valence state of Fe in 3+ state.

The reduction in mobile oxygen vacancies inhibits the diffusion of ions within the lattice and leads to decrease in the grain growth.[28] The decrease in grain size is also observed in the Sc substituted $Bi_{0.9}Nd_{0.1}FeO_3$ compound[11] and corroborates our observation. The co-substitution of Sm and Sc in BFO densifies the microstructure and reduces the porosity due to suppression in oxygen vacancies.

## Raman studies

The structural modifications, observed from XRD patterns, can also be analysed using Raman scattering spectra. The Raman spectra of BFO and BSFSO compounds are shown in Fig. 4. For the rhombohedral BFO with *R3c* space group, thirteen Raman modes ($4A_1+9E$) are possible.[29] For the present BFO compound, three $A_1$ modes at ($A_1$–1 =) 139 $cm^{-1}$, ($A_1$–2 =) 172 $cm^{-1}$, and ($A_1$–3 =) 231 $cm^{-1}$ and

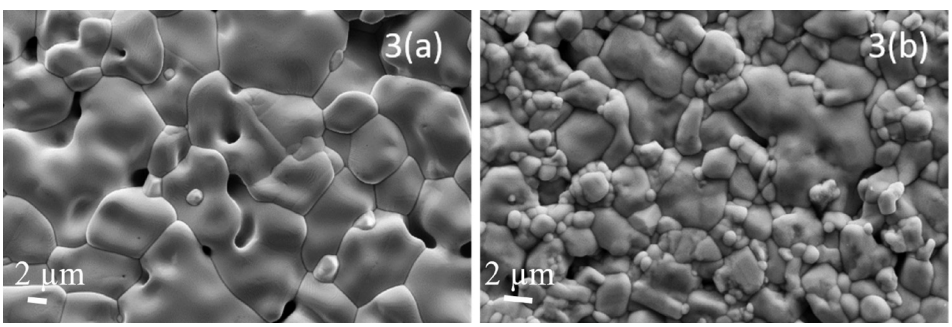


FIG. 3. FE-SEM micrographs of sintered (a) BFO and (b) BSFSO compounds.

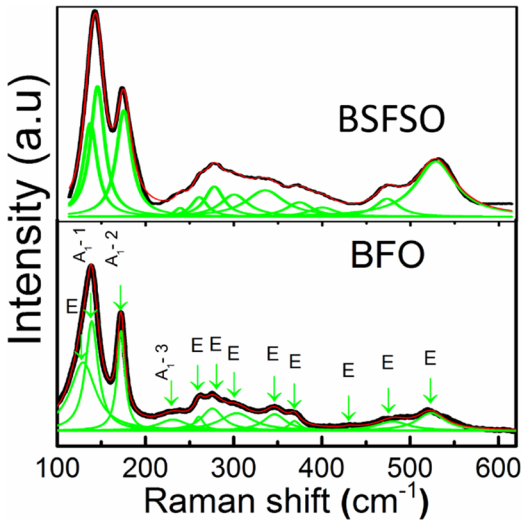


FIG. 4. Room temperature Raman spectra of BFO and BSFSO compounds (black) along with the fitted spectra (red) and decomposed active modes (green).

eight $E$ modes at 129, 261, 276, 346, 369, 432, 480, and 524 $cm^{-1}$ are observed. The $A_1$ modes of BFO at 139 $cm^{-1}$, 172 $cm^{-1}$, and 231 $cm^{-1}$ (which belong to Bi-O modes) show blue shift to 145 $cm^{-1}$, 176 $cm^{-1}$, and 239 $cm^{-1}$, respectively, in the BSFSO compound. The blue shift can be accounted due to the substitution of relatively heavier $Bi^{3+}$ ions by lighter $Sm^{3+}$ ions at the $A$-site as the frequency of the mode is proportional to $(k/M)^{1/2}$ (where $k$ is the force constant and $M$ is the reduced mass), provided it is governed by the local factors.[30] The $E$ mode at 276 $cm^{-1}$ in BFO shifts to 278 $cm^{-1}$ indicates destabilization of $B$-site cations due to the change in internal chemical pressure with the substitution of Sc which in turn causes octahedral tilts[8,31] and hence leads to the structural changes. The co-substitution of Sm and Sc causes disorder in their respective sites which are reflected in terms of increase in the FWHM of Raman modes. It is evidenced from the Raman spectra that the modes $A_1$–2, $A_1$–3, and $E$ mode at 261 $cm^{-1}$, which are corresponding to Bi-O bonds, show weaker scattering intensities in the BSFSO compound. The decrease in the intensity of these modes indicates a weakening of stereochemical activity of $6s^2$ lone pair electrons of $Bi^{3+}$ ions due to the substitution of $Sm^{3+}$ at the $A$-site of BFO.[32] The decline in stereochemical activity affects the long range of ferroelectric ordering and hence deteriorates the ferroelectric property of the compound. The same conclusion is also drawn from the XRD patterns.

The $E$ modes at 276 $cm^{-1}$ and 369 $cm^{-1}$ in BFO show red shift to 278 $cm^{-1}$ and 374 $cm^{-1}$, respectively, whereas the $E$ mode at 346 $cm^{-1}$ in BFO shows blue shift to 335 $cm^{-1}$ in the BSFSO compound. Such changes are attributed to the evolution of orthorhombic phase in the BSFSO compound,[33] which also corroborated our XRD findings.

## Magnetic properties

Isothermal magnetization ($M$) and magnetic field ($H$) curves of BFO and BSFSO compounds are shown in Fig. 5. In BFO, the $G$-type antiferromagnetic structure is superimposed

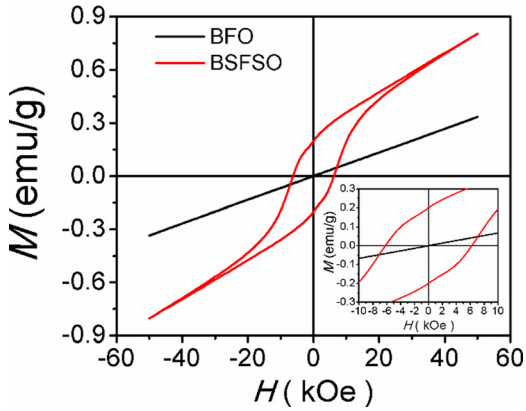


FIG. 5. Room temperature magnetic hysteresis curves of BFO and BSFSO compounds.

with a space modulated spin structure (SMSS) with an incommensurate wave length of 620 Å.[34] BFO shows a linear variation of magnetization with respect to the applied field with a remanent magnetization of ($M_r$ =) 0.0006 emu/g. The partial substitution of $Sm^{3+}$ for $Bi^{3+}$ and $Sc^{3+}$ for $Fe^{3+}$ ions significantly influences the magnetic behavior of BFO. An enhanced $M_r$ of 0.2 emu/g is observed in the BSFSO compound which is three orders of magnitude greater than that of BFO. The observed $M_r$ value is relatively higher than in (Ba, Zr), (Sm, Sc) co-substituted BFO compounds.[35,36] The improved magnetization could be attributed to (i) structural modification from rhombohedral to an orthorhombic structure and (ii) destruction of SMSS. As the structure of BSFSO compound changes to orthorhombic (with a phase fraction of 84%), the Fe-O-Fe bond angle (see Table I) changes towards 180°. In other words, straightening of Fe-O-Fe bond angle facilitates ferromagnetic interactions via oxygen, instead of conventional antiferromagnetic interaction.[37]

The coercive field $H_c$ of BFO and BSFSO compounds are 75 Oe and 6.2 kOe, respectively. The enhanced coercive field in the BSFSO compound may be due to the change in structural anisotropy in the compound.[11] The improved $H_c$ is explained using the formula

$$H_c = \frac{2K}{M}, \tag{3}$$

where $K$ is the total anisotropy and $M$ is the magnetization of the compound. The co-substitution enhances both structural anisotropy and magnetization in such a way that the ratio between them gives rise to an overall enhancement in $H_c$. Further, the enhanced coercive field is also attributed to decrease in grain size.[38] As the grain size of BSFSO compound is smaller than that of BFO, an increase in $H_c$ is expected which is consistent with our observation. Differential scanning calorimetry measurements are carried out to find the Neel temperature of the compounds (not shown here). The minimum of DSC curve of a compound corresponds to the antiferromagnetic to paramagnetic transitions ($T_N$) of that compound. The $T_N$ values of BFO and BSFSO compounds obtained from DSC plots are 373 and 354 °C, respectively. A decrease in $T_N$ with the substitution can also be found in the literature.[39]

### Impedance studies

Impedance spectroscopy (IS) is a non-destructive technique which can be used to analyse the insulating character of the compounds.[40] The frequency variation of real part of impedance (Z′) and imaginary part of impedance (Z″) is measured in the temperature range 30 °C to 300 °C for both the compounds. (However, data are presented for limited temperatures.) In order to study the contribution of grain and grain boundary resistances to the electrical resistivity of the compound, Nyquist plots (i.e., Z″ vs Z′) are plotted from 165 °C to 225 °C as shown in Fig. 6.

It is observed that above 150 °C, two semi-circular arcs are observed. The high frequency semi-circular arc corresponds to the grain and the low frequency semi-circular arc corresponds to grain boundary effects.[41] The two semi-circular arcs in the Nyquist plots, corresponding to both grain and grain boundary, can be modelled using two *RC* parallel circuits. The grain resistance $R_g$ and grain boundary resistance $R_{gb}$ are estimated by fitting the data using the equivalent circuit model, and the values are given in Table II. The grain and grain boundary resistances are enhanced by one order in the BSFSO compound which indicates that Sm and Sc co-substitution enhances the electrical resistivity of BFO. Further, grain boundary resistances are dominated over grain resistances in both the compounds indicating that the major contribution to the electrical resistivity is from grain boundaries. As discussed from microstructural measurements, it can be concluded that the increase in $R_g$ and $R_{gb}$ could be due to the decrease in oxygen vacancies in the BSFSO compound. In addition to this, the increase in resistance may also be due to the structural change in the BSFSO compound which may promote high resistance path for the movement of charge carriers.

### Electric modulus

The electrical response of a material can also be studied using electric modulus formalism. The value of imaginary part of electric modulus ($M''$) is calculated using the formula

$$M'' = \omega C_o Z', \tag{4}$$

where $\omega$ is the angular frequency and $C_o$ is the empty capacitance. The frequency variation of $M''$ for BFO and BSFSO compounds is shown in Fig. 7. As the frequency increases, $M''$ increases, shows a maximum value ($M''_{max}$) at a particular frequency ($\omega_{max}$), and then decreases. The temperature variation of $\omega_{max}$ follows the Arrhenius law

$$\omega_{max} = \omega_o e^{-E/kT}, \tag{5}$$

where $\omega_o$ is a constant and $E$ is the activation energy. The data are fitted with Eq. (5) and the activation energies obtained are 0.69 and 0.96 eV for BFO and BSFSO compounds, respectively. Further, the value of $M''$ at $\omega_{max}$ can be expressed as

$$M'' = \frac{\varepsilon_o}{2C}, \tag{6}$$

where $C$ is the capacitance. It is evidenced from Fig. 7 that the value of $M''$ for BFO is smaller than that of the BSFSO compound which indicates the decrease in the dielectric constant of the BSFSO compound. The decrease in the dielectric constant (data not presented here) in BSFSO compounds is also consistent with our observation. The presence of oxygen vacancies causes increased hopping conductivity which in turn increases the dielectric constant. The decrease in the dielectric constant in the BSFSO compound indicates the reduction of the oxygen vacancies upon substitution.[31] The reduction of oxygen vacancies with the substitution of Sm and Sc in BFO is anticipated because of stronger bond enthalpy of Sm-O and Sc-O bonds, respectively, than that of Bi-O and Fe-O bonds.[26]

TABLE II. Grain resistance and grain boundary resistances of BFO and BSFSO compounds at different temperatures.

| | BFO | | BSFSO | |
|---|---|---|---|---|
| Temperature (°C) | $R_g$ (MΩ) | $R_{gb}$ (MΩ) | $R_g$ (MΩ) | $R_{gb}$ (MΩ) |
| 165 | 0.44 | 3.26 | 7.25 | 47.10 |
| 180 | 0.23 | 1.51 | 6.00 | 21.27 |
| 195 | 0.12 | 0.59 | 4.46 | 7.85 |
| 210 | 0.06 | 0.22 | 1.70 | 5.65 |
| 225 | 0.04 | 0.11 | 0.89 | 2.61 |
| 240 | 0.02 | 0.05 | 0.60 | 0.71 |

### Leakage current measurements

Leakage current ($J$) – electric field ($E$) curves of BFO and BSFSO compounds are shown in Fig. 8. The leakage current density in BFO is observed to be decreased by one order with the co-substitution which can be explained as

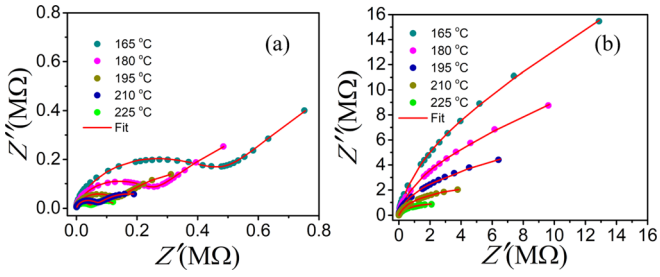


FIG. 6. Nyquist plots for (a) BFO and (b) BSFSO compounds between 165 °C to 225 °C. Solid circles represent data and red lines represent fitted data at different temperatures.

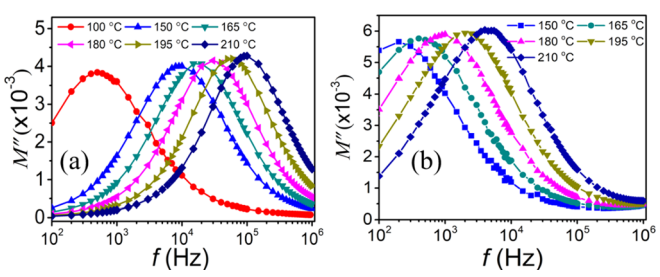


FIG. 7. Frequency variation of imaginary part of $M''$ at different temperatures. Symbols represent data and lines represent fitted data at different temperatures.

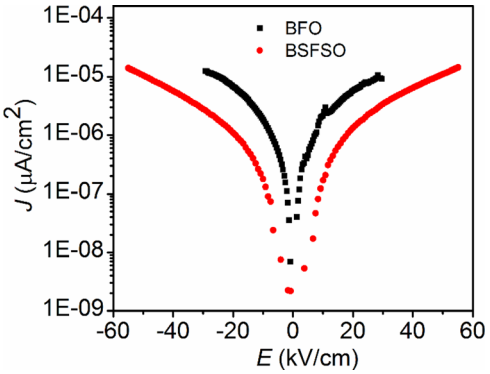


FIG. 8. Leakage current density vs electric field (*J*-*E*) curves of BFO and BSFSO curves.

follows. The oxygen vacancy movements are considered as prime source of leakage currents in BFO.[42] The electric field produces oxygen vacancies if its strength is high enough to dissociate the bonds between the cations (in this case $Bi^{3+}$/$Sm^{3+}$ and $Fe^{3+}$/$Sc^{3+}$) and $O^{-2}$ ions. As the bond enthalpies of Bi-O and Fe-O bonds are, respectively, weaker than that of Sm-O and Sc-O bonds, more oxygen vacancies are produced in the BFO compared to that in the BSFSO compound under the application of the same electric field.

In other words, under the influence of same field strengths, the leakage current density is smaller in the BSFSO compound than in BFO which is also consistent with our observation. In addition to this, the reduction of leakage current density could be due to the decrease in grain size. The decrease in grain size leads to the increase in grain boundaries which act as scattering centers for the charge carriers and hence the reduction of leakage current density in the BSFSO compound. The increase in the grain boundary resistance is also observed in the BSFSO compound from impedance studies.

## CONCLUSIONS

The polycrystalline $BiFeO_3$ (BFO) and $Bi_{0.85}Sm_{0.15}Fe_{0.90}Sc_{0.10}O_3$ (BSFSO) ceramics were synthesized by conventional solid-state route. An evolution of orthorhombic *Pnma* structure with a phase fraction of 84% was observed along with 16% phase fraction of the rhombohedral *R3c* structure upon the co-substitution of Sm and Sc in BFO. Raman measurements also corroborated the evolution of orthorhombic structure in the substituted compound. The co-substitution decreased the grain size, reduced the porosity, and improved the density due to the suppression of the oxygen vacancy content in the BSFSO compound. Enhanced magnetization and improved coercive field were observed in the BSFSO compound and attributed to the destruction of the canted spin structure. A decrease in Neel temperature of nearly 20 °C is observed in the BSFSO compound. The reduction of oxygen vacancies was the prime cause for the observations: (i) decrease in dielectric constant, (ii) improved grain and grain boundaries resistances, and (iii) reduction in leakage current density in the substituted compound. A strong correlation between the structural, microstructural, magnetic, dielectric, and electrical properties of the compounds was established in the studied compounds.

## ACKNOWLEDGMENTS

S.A. gratefully acknowledges the financial support from the Department of Science and Technology (DST), India, to carry out this work, under the Project No. EMR/2014/000761.

[1]G. A. Smolenskii, V. M. Yudin, E. S. Sher, and Y. E. Stolypin, Sov. Phys. J. Exp. Theor. Phys. **16**, 622–624 (1963).
[2]W. Eerenstein, N. D. Mathur, and J. F. Scot, Nature **442**, 752–759 (2006).
[3]G. R. Blake, L. C. Chapon, P. G. Radaelli, S. Park, N. Hur, S. W. Cheong, and J. Rodriguez-Carvajal, Phys. Rev. B **71**, 214402 (2005).
[4]J. H. Lee, P. Murugavel, D. Lee, T. W. Noh, Y. Jo, M. H. Jung, K. H. Jang, and J. G. Park, Appl. Phys. Lett. **90**, 012903 (2007).
[5]G. Catalan and J. F. Scott, Adv. Mater. **21**, 2463–2485 (2009).
[6]M. Fiebig, J. Phys. D: Appl. Phys. **38**, R123 (2005).
[7]C. Ederer and N. A. Spaldin, Phys. Rev. B **71**, 060401 (2005).
[8]T. D. Rao, S. Asthana, and M. K. Niranjan, J. Alloys Compd. **642**, 192–199 (2015).
[9]Y. Zhang, S. Yu, and J. Cheng, J. Europ. Ceram. Soc. **30**, 271–275 (2010).
[10]T. D. Rao, A. Kumari, M. K. Niranjan, and S. Asthana, Phys. B: Condens. Matter. **448**, 267–272 (2014).
[11]T. D. Rao and S. Asthana, J. Appl. Phys. **116**, 164102 (2014).
[12]T. D. Rao, R. Ranjith, and S. Asthana, J. Appl. Phys. **115**, 124110 (2014).
[13]H. Dai, Z. Chen, R. Xue, T. Li, H. liu, and Y. Wang, Appl. Phys. A **111**(3), 907–912 (2013).
[14]V. A. Khomchenko, V. V. Shvartsman, P. Borisov, W. Kleemann, D. A. Kiselev, I. K. Bdikin, J. M. Vieira, and A. L. Kholkin, Acta Mater. **57**, 5137–5145 (2009).
[15]P. Suresh, P. D. Babu, and S. Srinath, J. Appl. Phys. **115**, 17D905 (2014).
[16]K. S. Nalwa and A. Garg, J. Appl. Phys. **103**, 044101 (2008).
[17]J. H. Lee, M. A. Oak, H. J. Choi, J. Y. Sonc, and H. M. Jang, J. Mater. Chem. **22**, 1667–1672 (2012).
[18]M. Kumar and K. L. Yadav, J. Appl. Phys. **100**, 074111 (2006).
[19]V. R. Reddy, D. Kothari, A. Gupta, and S. M. Gupta, Appl. Phys. Lett. **94**, 082505 (2009).
[20]Reetu, A. Agarwal, S. Sanghi, and N. Ahlawat, J. Phys, D: Appl. Phys. **45**, 165001 (2012).
[21]R. C. Lennox, M. C. Price, W. Jamieson, M. Jura, A. Daoud-Aladine, C. A. Murray, C. Tang, and D. C. Arnold, J. Mater. Chem. C **2**, 3345–3360 (2014).
[22]Z. Xing, X. Zhu, J. Zhu, and Z. Liu, J. Amer. Ceram. Soc. **97**, 2323–2330 (2014).
[23]Y. Gu, J. Zhao, W. Zhang, H. Zheng, L. Liu, and W. Chen, Ceram. Int. **43**, 14666–14671 (2017).
[24]I. O. Troyanchuk, D. V. Karpinsky, and M. V. Bushinsky, Phys. Rev. B **83**, 054109 (2011).
[25]A. K. Ghosh, G. D. Dwivedi, B. Chatterjee, and B. Rana, Solid State Commun. **166**, 22–26 (2013).
[26]Z. Qiang, X. Zhu, Y. Xu, H. Gao, and Y. Xiao, J. Alloys Compd. **546**, 57–62 (2013).
[27]JA. Kerr, *CRC Handbook of Chemistry and Physics*, 81st ed. (CRC Press, Boca Raton, Florida, USA, 2000).
[28]C. F. Chung, J. P. Lin, and J. M. Wu, Appl. Phys. Lett. **88**, 242909 (2006).
[29]H. Fukumura, H. Harima, K. Kisoda, and M. Tamada, J. Magn. Magn. Mater. **310**, e367–e369 (2007).
[30]D. Wu, Y. Deng, C. L. Mak, K. H. Wong, A. D. Li, M. S. Zhang, and N. B. Ming, Appl. Phys. A **80**, 607 (2005).
[31]Y. Yang, L. G. Bai, K. Zhu, Y. L. Liu, S. Jiang, J. Liu, J. Chen, and X. R. Xing, J. Phys.: Condens. Matter **21**, 385901 (2009).
[32]G. L. Yuan, S. W. Or, and H. L. W. Chan, J. Appl. Phys. **101**, 064101 (2007).
[33]Y. A. Zheng, Y. J. Wu, Z. X. Qin, and X. J. Chen, Chin. J. Chem. Phys. **26**(2), 157 (2013).
[34]I. Sosnowska, T. Peterlin-Neumaier, and E. Steichele, J. Phys. C: Solid State Phys. **15**, 4835 (1982).
[35]S. M. Abdul Kader, D. E. Jain Ruth, M. V. G. Babu, M. Muneeswaran, N. V. Giridharan, and B. Sundarakannan, Ceram. Int. **43**, 15544–15550 (2017).
[36]C. Wang, L. Yang, Z. Li, M. Zeng, A. Zhang, M. Qin, X. Lu, X. Gao, J. Gao, and K. H. Lam, Ceram. Int. **43**, 12764–12769 (2017).

[37]J. Wei, R. Haumont, R. Jarrier, P. Berhtet, and B. Dkhil, Appl. Phys. Lett. **96**, 102509 (2010).
[38]L. Zhai, Y. G. Shi, S. L. Tang, L. Y. Lv, and Y. W. Du, J. Phys. D: Appl. Phys. **42**, 165004 (2009).
[39]D. Kothari, V. R. Reddy, A. Gupta, C. Meneghini, and G. Aquilanti, J. Phys.: Condens. Matter **22**, 356001 (2010).
[40]M. Li, A. Feteira, M. Mirsaneh, S. Lee, M. T. Lanagan, C. A. Randall, and D. C. Sinclair, J. Am. Ceram. Soc. **93**, 4087 (2010).
[41]J. R. Macdonald, *Impedance Spectroscopy* (John Wiley and Sons, New York, 1987), Chap. 4.
[42]X. D. Qi, J. G. Dho, R. Tomov, M. G. Blamire, and J. L. MacManus-Driscoll, Appl. Phys. Lett. **86**, 062903 (2005).